Article

Journal of
Nanoscience and Nanotechnology
Vol. 18, 7554–7556, 2018
www.aspbs.com/jnn

Single-Mode Surface Emitting Terahertz Quantum Cascade Lasers

Y. Y. Li[1,2], F. Y. Zhao[1,2], J. Q. Liu[1,2,*], F. Q. Liu[1,2,*], J. C. Zhang[1], N. Zhuo[1], S. Q. Zhai[1], L. J. Wang[1,2], S. M. Liu[1,2], and Z. G. Wang[1,2]

[1] *Key Laboratory of Semiconductor Materials Science, Institute of Semiconductors, Chinese Academy of Sciences, and Beijing Key Laboratory of Low Dimensional Semiconductor Materials and Devices, Beijing 100083, China*
[2] *College of Materials Science and Opto-Electronic Technology, University of Chinese Academy of Sciences, Beijing 101408, China*

We present second-order grating surface-emitting terahertz quantum cascade lasers based on metal–metal waveguides. A maximum peak power of 12.2 mW is realized at 5 K in the pulsed mode, and the maximum operation temperature is 105 K. Stable single-mode emissions at ~89 μm with a side-mode suppression ration at about 25 dB is achieved at all operating conditions. By inserting a central π-phase shift in the device, a single-lobed far-field radiation pattern is obtained with a small divergence angle of 4° in the cavity-length direction.

Keywords: Terahertz, Quantum Cascade Lasers, Single-Mode, Distributed Feedback Gratings.

1. INTRODUCTION

Terahertz (THz) quantum cascade lasers (QCLs) have been one of the most potential solid sources in the terahertz region during decades of development. For a variety of applications, such as local oscillators, THz spectroscopy, wireless communication[1–3] and stable single-mode emissions with a good beam pattern is highly desired. Nowadays, the commonly employed solution for realizing single-mode emission is fabricating distributed feedback (DFB) gratings on the surface of the devices.[4–7] For semi-insulating surface-plasmon (SISP) waveguides, a first-order DFB grating edge-emitting structure is preferred, rather than a second-order DFB grating surface-emitting structure due to the small light confinement factor that results in a low surface extraction efficiency.[8] However, the radiation from the facet always presents a double-lobed beam pattern because of the leakage mode in the SI-GaAs substrate.[8] The only method to improve the pattern shape without external instruments is defining the slit-grating plasmonic collimator on the output facet,[9,10] but it is very difficult in processing. Compared with SISP waveguides, metal–metal (MM) waveguides provide strong mode confinement, resulting in a high surface extraction efficiency and high operating temperatures.[8] Using monolithic integrated second-order grating structures, surface-emitting perpendicular to the plane is feasible, which is provided by the first-order diffraction of the second-order DFB gratings.[11]

There are two classes of modes at the band-edge states within the second-order grating surface-emitting mechanism: the anti-symmetric and symmetric mode. These two modes have similar material and cavity losses, but exhibit significantly different radiative losses. The anti-symmetric mode, which has lower radiative loss than the symmetric mode in a finite-size device, is normally favorable to lasing due to the lower total losses. However, the anti-symmetric mode lasing generally leads to a double-lobed far-field pattern along the cavity-length direction.[12] The simplest method to improve the beam pattern is inserting a central π-phase shift in the cavity to make the field distribution symmetric with respect to the center of the device.[13–15] This solution enables a single-lobed beam pattern.

In this paper, we present high-performance operation of surface-emitting second-order grating THz QCLs with a central π-phase shift based on metal–metal waveguides. A maximum peak power of 12.2 mW is realized at 5 K in a pulsed mode, and the device lases up to 105 K. Stable single-mode emission at ~89 μm with a side-mode suppression ration (SMSR) at about 25 dB is achieved at all operating conditions. Due to the central π-phase shift in the cavity, single-lobed far-field radiation patterns are obtained with a small divergence angle of 4° in the cavity-length direction.

*Authors to whom correspondence should be addressed.

1533-4880/2018/18/7554/003 doi:10.1166/jnn.2018.16061

2. DEVICE DESIGN AND FABRICATION

The grating periods of $\Lambda = \lambda/n_{\text{eff}} = 25$ μm were defined with the calculated effective index $n = 3.5$ and central wavelength 87.7 μm. To obtain a stable single-mode, we simulated the second-order grating structure with different grating duty cycles σ based on the finite-element method with periodical boundary conditions to find the optimal grating design. In Figure 1, the results are plotted with a constant grating depth $d = 350$ nm (etching the top highly-doped GaAs layer completely) and various duty cycles σ. There exists two modes, anti-symmetric mode (mode 1) and symmetric mode (mode 2), in the active region which are located beneath the grating peak and slit, respectively. As presented in Figure 1, the coupling coefficient gets the maximum value at $\sigma = 0.95$. In addition, both the largest losses difference between the two modes and the minimum value of losses for anti-symmetric mode appear at $\sigma = 0.85$. Thus, the anti-symmetric mode is favorable to lasing, and the far-field radiation pattern is predominantly two-lobed with a null in the center. Considering a compromise between coupling coefficient and losses, 2.5-μm-wide slits were selected, i.e., duty cycle of 90% was obtained corresponding to grating period $\Lambda = 25$ μm. In addition, we employed a central π-phase shift in the grating region to flip the phase of emission from all slits in one half of the grating region by π with respect to the other half to enable a single-lobed beam pattern.

The material structure was grown by EPI GENII solid source molecular beam epitaxy (MBE) system on a SI-GaAs substrate. After a 150-nm-thick $Al_{0.5}Ga_{0.5}As$ etch-stop layer, a 150 nm highly-doped (Si, 2.5×10^{18} cm^{-3}) GaAs layer was grown, followed by the active core, which was composed of 185 periods of $Al_{0.15}Ga_{0.85}As$/GaAs heterostructure that is similar to that in Ref. [16]. The growth was concluded by a 100 nm (Si, 5×10^{18} cm^{-3}) GaAs layer that was highly-doped.

The fabrication of metal–metal waveguides was followed using an In–Au thermoscopression method.[17] Bonding took place at approximately 250 °C as pressure to the stack was applied for 15 minutes. Then, the substrate was removed via lapping and selective etching with NH_4OH:H_2O_2 (1:19 v/v). The $Al_{0.5}Ga_{0.5}As$ etch stop layer was removed by immersion in 48% HF acid for 1 minutes. After that, the gratings were defined followed by metal deposition (Ti/Au) and lift-off. Wet chemical etching was employed to remove the highly-doped GaAs layer in the slits entirely and smooth the grating grooves. Finally, the ridges were formed by optical lithography and inductively coupled plasma reactive ion etching. The top doped GaAs contact layer was left at each end of the ridges and also along the sides of the grating to provide absorbing boundary conditions. After polishing and back-contact deposition, the laser chips were cleaved into 150-μm-wide and 1-mm-long devices.

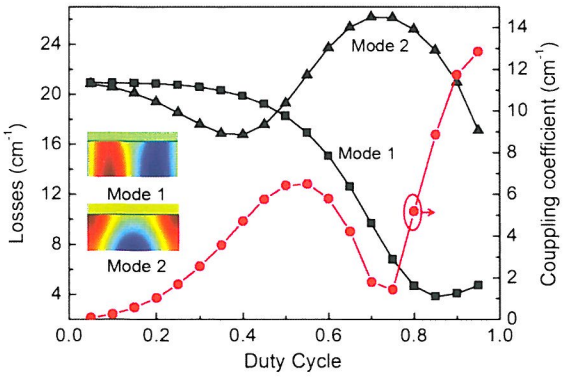

Figure 1. The simulated coupling coefficient and losses of the band-edge modes as function of grating duty cycle σ.

3. RESULTS AND DISCUSSION

The devices were indium-soldered onto copper mounts for characterization in a helium cryostat. The powers were collected by an absolute THz power meter and not corrected by the transmission of the polyethylene window. The measurement of the lasing spectra was operated through a Fourier-transform infrared spectrometer with a resolution of 0.5 cm^{-1} in rapid scan mode. The beam divergence measurement was done by placing a Golay cell detector on a 15-cm-radius sphere centered on the emission facet to collect lasing light with a resolution of 0.5°. All pulsed measurements were performed at a 5 kHz repetition rate with a pulse of 2 μs.

Figure 2 shows the lasing spectra of a surface-emitting DFB device and a normal Fabry-Perol (F-P) device at 5 K when they reach the maximum power. The spectrum of the F-P device centers at ~87.7 μm and the DFB device lases at ~89 μm with the SMSR of ~25 dB. Stable single-mode emission is realized at all operating conditions. The refractive index of the active region is extracted to be 3.56, which is very close to the calculated value.

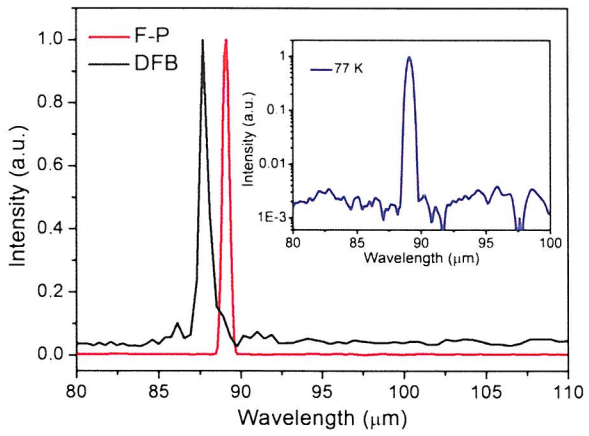

Figure 2. The lasing spectra of the surface-emitting DFB device and normal Fabry-Perol (F-P) device at 5 K. The inset shows the lasing spectrum of the DFB device at 77 K.

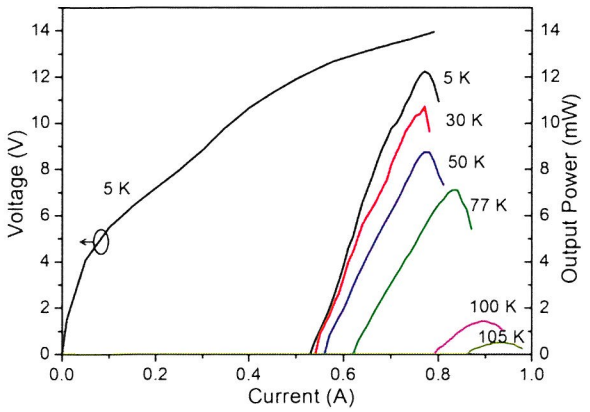

Figure 3. The typical light–current–voltage (L–I–V) characteristics of the single-mode device in pulsed mode.

The inset shows the lasing spectrum of the DFB device in logarithmic scale at 77 K.

Figure 3 presents the typical pulsed light–current–voltage (L–I–V) characteristics of the single-mode DFB device at different heat sink temperatures from 5 K to 105 K. The maximum peak power of 12.2 mW is realized at 5 K with a threshold current density of 360 A/cm^2 and a maximum slope efficiency of 60.4 mW/A. Higher power may be obtained by choosing a more appropriate grating period to shift the emission wavelength to the center of the gain spectrum. The maximum optical power of 0.5 mW is still obtained at 105 K with a threshold current density of 580 A/cm^2 and a maximum slope efficiency of 5.9 mW/A.

Figure 4 shows the normalized beam pattern of the device in pulsed operation at 77 K. Due to the insertion of central π-phase shift, a single-lobed pattern is observed in the direction along the cavity-length with a full width at half maximum (FWHM) of 4°. On the other hand, the beam in the ridge-width direction is relatively divergent with a FWHM of 43° due to the waveguide width being in the order of the wavelength. Concentric-circular-grating design may further optimize the far-field beam pattern.

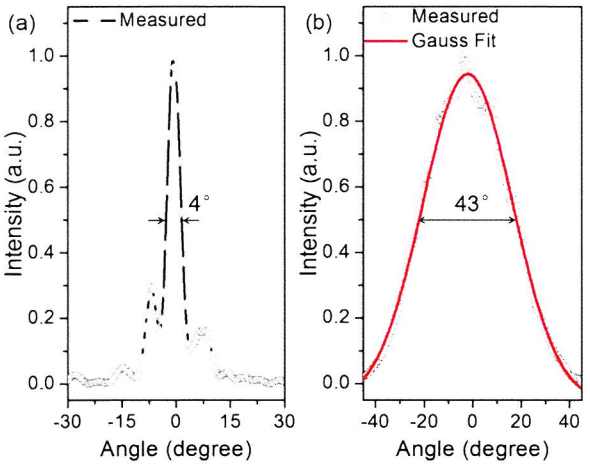

Figure 4. (a) The far-field beam pattern in cavity-length direction of the single-mode device in pulsed operation at 77 K. (b) The far-field beam pattern in ridge-width direction of the single-mode device.

4. CONCLUSION

In conclusion, we report high performance surface-emitting THz QCLs at ~89 μm. Peak power of 12.2 mW is realized in pulsed mode with a maximum slope efficiency of 60.4 mW/A at 5 K. The device can lase up to 105 K with 0.5 mW. Stable single-mode emission with a SMSR of ~25 dB is achieved under all operating conditions. Single-lobed far-field beam patterns with a small divergence of 4° in the cavity-length direction are also observed by inserting a central π-phase shift in the cavity.

Acknowledgments: This work was partially funded by the National Key R&D Program of China (Grant No. 2016YFB0402303), National Natural Science Foundation of China (Grant Nos. 61734006, 61674144, 61774146, 61504135, 61627822, 61404131, 61435014, 61574136), Key Projects of Chinese Academy of Sciences (Grant Nos. ZDRW-XH-2016-4, QYZDJ-SSW-JSC027). The authors would like to acknowledge P. Ling and Y. Hu for the help of device fabrication.

References and Notes

1. J. L. Kloosterman, D. J. Hayton, Y. Ren, T. Y. Kao, J. N. Hovenier, J. R. Gao, T. M. Klapwijk, Q. Hu, C. K. Walker, and J. L. Reno, *App. Phys. Lett.* 102, 011123 (**2013**).
2. T. Hagelschuer, M. Wienold, H. Richter, L. Schrottke, H. T. Grahn, and H. W. Hubers, *IEEE Opt. Express* 25, 30203 (**2017**).
3. M. Tonouchi, *Nature Photon.* 1, 97 (**2007**).
4. T. Wang, J. Q. Liu, Y. F. Li, J. Y. Chen, F. Q. Liu, L. J. Wang, J. C. Zhang, and Z. G. Wang, *IEEE Electron. Dev. Lett.* 34, 1412 (**2013**).
5. T. Y. Kao, Q. Hu, and J. L. Reno, *IEEE Opt. Lett.* 37, 2070 (**2012**).
6. G. Xu, R. Colombelli, S. P. Khanna, A. Belarouci, X. Letartre, L. Li, E. H. Linfield, A. G. Davies, H. E. Beere, and D. A. Ritchie, *Nat. Commun.* 3, 952 (**2012**).
7. C. Wu, S. Khanal, J. L. Reno, and S. Kumar, *Optica* 3, 734 (**2016**).
8. B. S. Williams, *Nature Photon.* 1, 517 (**2007**).
9. N. Yu, Q. J. Wang, M. A. Kats, J. A. Fan, S. P. Khanna, L. Li, A. G. Davies, E. H. Linfield, and F. Capasso, *Nature Mater.* 9, 730 (**2010**).
10. N. Yu, J. Fan, Q. J. Wang, C. Pflugl, L. Diehl, T. Edamura, M. Yamanishi, H. Kan, and F. Capasso, *Nature Photon.* 2, 564 (**2008**).
11. R. F. Kazarinov and C. H. Henry, *IEEE J. Quantum Electron.* QE-21, 144 (**1985**).
12. S. Kumar, B. S. Williams, Q. Qin, A. W. M. Lee, and Q. Hu, *IEEE Opt. Express* 15, 113 (**2007**).
13. S. Li, G. Witjaksono, S. Macomber, and D. Botez, *IEEE J. Sel. Top. Quan. Electron.* 9, 1153 (**2003**).
14. G. Witjaksono, S. Li, J. J. Lee, D. Botez, and W. K. Chan, *App. Phys. Lett.* 83, 5365 (**2003**).
15. E. Miyai and S. Noda, *Appl. Phys. Lett.* 86, 111113 (**2005**).
16. Y. Y. Li, J. Q. Liu, F. Q. Liu, J. C. Zhang, S. Q. Zhai, N. Zhuo, L. J. Wang, S. M. Liu, and Z. G. Wang, *Chin. Phys. B* 25, 084206 (**2016**).
17. B. S. Williams, S. Kumar, H. Callebaut, and Q. Hu, *Appl. Phys. Lett.* 83, 2124 (**2003**).

Received: 3 January 2018. Accepted: 22 March 2018.